# Pacemaker Synchronization of Electrically Coupled Rabbit Sinoatrial Node Cells

E. Etienne Verheijck,*‡ Ronald Wilders,*‡ Ronald W. Joyner,§ David A. Golod,§ Rajiv Kumar,§ Habo J. Jongsma,‡ Lennart N. Bouman,* and Antoni C.G. van Ginneken*

From the *Academic Medical Center, University of Amsterdam, Department of Physiology, 1100 DE Amsterdam, The Netherlands; ‡Department of Medical Physiology and Sports Medicine, Utrecht University, 3584 CG Utrecht, The Netherlands; and §Todd Franklin Cardiac Research Laboratory, The Children's Heart Center, Department of Pediatrics, Emory University, Atlanta, Georgia 30322

ABSTRACT The effects of intercellular coupling conductance on the activity of two electrically coupled isolated rabbit sinoatrial nodal cells were investigated. A computer-controlled version of the "coupling clamp" technique was used in which isolated sinoatrial nodal cells, not physically in contact with each other, were electrically coupled at various values of ohmic coupling conductance, mimicking the effects of mutual interaction by electrical coupling through gap junctional channels. We demonstrate the existence of four types of electrical behavior of coupled spontaneously active cells. As the coupling conductance is progressively increased, the cells exhibit: (*a*) independent pacemaking at low coupling conductances, (*b*) complex dynamics of activity with mutual interactions, (*c*) entrainment of action potential frequency at a 1:1 ratio with different action potential waveforms, and (*d*) entrainment of action potentials at the same frequency of activation and virtually identical action potential waveforms. The critical value of coupling conductance required for 1:1 frequency entrainment was <0.5 nS in each of the five cell pairs studied. The common interbeat interval at a relatively high coupling conductance (10 nS), which is sufficient to produce entrainment of frequency and also identical action potential waveforms, is determined most by the intrinsically faster pacemaker cell and it can be predicted from the diastolic depolarization times of both cells. Evidence is provided that, at low coupling conductances, mutual pacemaker synchronization results mainly from the phase-resetting effects of the action potential of one cell on the depolarization phase of the other. At high coupling conductances, the tonic, diastolic interactions become more important.

KEY WORDS: action potentials • electrophysiology • coupling clamp • gap junctions • perforated patch clamp

## INTRODUCTION

In the sinoatrial (SA)[1] node synchronization of the activation of electrically coupled, spontaneously pacing cells is a required attribute of normal action potential initiation. Individual isolated SA nodal cells display a large variety in action potential waveforms (Nakayama et al., 1984; Bouman and Jongsma, 1986, 1995). Moreover, individual cells may have irregular firing patterns, with a varying cycle length (Opthof, 1988; Wilders and Jongsma, 1993), which is most likely due to differences in the composition of membrane currents (Nathan, 1986; Honjo et al., 1996). For the SA node to maintain a stable and regular discharge pattern, individual cells have to interact electrically such that their activation times are synchronized, producing action potentials at a regular rate. The mechanisms by which cells with different intrinsic rates of automaticity maintain this synchronization has been the subject of numerous studies using a variety of experimental and model systems.

Several experimental approaches have been used to study the electrical interactions between cardiac cells as a function of intercellular conductance without the complexity of a multidimensional syncytium. Studies using thin SA node strips (Jalife, 1984; Delmar et al., 1986), with the central region of the strip sealed off in a compartment containing either ion-free sucrose solution or Tyrode solution containing heptanol, showed synchronization of the proximal and distal regions of the strand after electrical coupling had been established. However, specific measurements of cellular properties could not be made with this "sucrose gap" technique, because the tissue on either side of the gap was not isopotential. Other studies have used aggregates of spontaneously beating chick embryonic heart cells (Clapham et al., 1980; Scott, 1979) and showed synchronization of the aggregates after electrical coupling had been established between the two aggregates. Studies on cultured, spontaneously beating neonatal rat and embryonic chick heart cells have shown that

Address correspondence to Dr. E. Etienne Verheijck, Academic Medical Center, University of Amsterdam, Department of Physiology, PO Box 22700, 1100 DE Amsterdam, The Netherlands. Fax: 31 20 6919319; E-mail: e.verheijck@amc.uva.nl

[1]*Abbreviations used in this paper:* $APD_{50}$, action potential duration at 50% repolarization; DDR, diastolic depolarization rate; DDT, diastolic depolarization time; $G_c$, coupling conductance; IBI, interbeat interval; $I_c$, coupling current; $I_{cap}$, capacitative current; $I_{ion}$, membrane ionic current; KB, Kraft-Brühe; SA, sinoatrial.


J. Gen. Physiol. © The Rockefeller University Press • 0022-1295/98/01/95/18 $2.00
Volume 111 January 1998 95–112
http://www.jgp.org

beating irregularity decreases when more cells become coupled (Ypey et al., 1979; Jongsma et al., 1983). Clay and DeHaan (1979) showed that the coefficient of variation of the interbeat interval of embryonic chick ventricular cell aggregates was inversely proportional to the square root of the number of interconnected cells. Wilders (1993) reached the same conclusion in a model study on SA nodal cells of the rabbit.

Several attempts have been made to estimate the minimal amount of coupling conductance required for pacemaker synchronization. Anumonwo et al. (1992) observed a single-channel junctional conductance of ~50 pS in SA node cell pairs. Using this value, they estimated that approximately three gap junction channels between the cells would allow pacemaker synchronization. In a model study, Cai et al. (1994) determined that approximately four gap junction channels of 50 pS are needed for frequency entrainment. In a previous study (Wilders et al., 1996) in which we electrically coupled an SA node cell to the Wilders-Jongsma-van Ginneken model of an SA node cell (Wilders et al., 1991), we showed that the critical amount of coupling depends on the difference in the intrinsic interbeat interval of both cells. At an interbeat interval difference of ~10%, the critical coupling conductance became as low as 75 pS. Calculations performed by Noble (appendix to DeHaan, 1982) also indicate that two cells pacing at different frequencies could synchronize when connected by a gap junctional conductance of 100 pS.

We previously described an experimental "coupling clamp" system in which two isolated cells, not in physical contact with each other, can be electrically coupled at any desired value of intercellular conductance by means of an external circuit that continuously applies time-varying currents to each cell with a sign and magnitude that would have been present if the cells had been physically coupled (Tan and Joyner, 1990). The coupling clamp system allows the rapid independent measurement of the intrinsic cellular properties, and then the analysis of the effects of a wide range of intercellular conductance values on the electrical behavior of the cell pairs. In the present study, we have used a digital version of the coupling clamp technique to couple two real, freshly isolated SA node cells over a range of coupling conductances. Using this new coupling clamp technique, we determine the required coupling conductance for synchronization and the electrical behavior of these spontaneously active cells when coupled at levels below that for which complete synchronization occurs. We provide evidence that, at low coupling conductances, mutual pacemaker synchronization results mainly from the phase resetting effects of the action potential of one cell on the depolarization phase of the other. At higher coupling conductances, the tonic, diastolic interaction prevails.

## MATERIALS AND METHODS

### *Cell Isolation and Electrodes*

Single SA nodal myocytes were isolated according to the method of DiFrancesco et al. (1986), with some modifications, as previously described in detail (Verheijck et al., 1995). Briefly, New Zealand albino rabbits of either sex weighing 1.8–2.5 kg were anaesthetized with 1 mg/kg Hypnorm (0.32 mg/ml fentanyl citrate and 10 mg/ml fluanisone, intramuscular; Janssen Pharmaceuticals, Tilburg, The Netherlands) under artificial ventilation. The thorax was opened and 0.1 ml heparin sodium (5,000 IU/ml) was injected into the left ventricle. The heart was excised and mounted on a Langendorff perfusion system. Blood was washed out with oxygenated normal Tyrode solution at 37°C for 10 min. Next, the heart was perfused with nominally $Ca^{2+}$-free Tyrode solution for 5 min. The SA node area was excised and pinned down on a Sylgard layer in a Petri dish containing nominally $Ca^{2+}$-free Tyrode solution. Subsequently, the SA node was cut into four strips (width ~1 mm, length ~2 mm) perpendicular to the crista terminalis. The strips were placed in a test tube containing oxygenated nominally $Ca^{2+}$-free Tyrode solution at 37°C. The solution was refreshed two times. Next, the strips were incubated in 10 ml of enzyme solution at 37°C for 10–14 min. During the incubation, the strips were gently triturated through a pipette with a tip diameter of 2.3 mm. At regular intervals, the solution was microscopically examined for the presence of dissociated myocytes. When single cells appeared, the strips were immediately transferred into a modified "Kraft-Brühe" (KB) solution (Isenberg and Klockner, 1982) and gently shaken. The modified KB solution was refreshed three times to remove the dissociation solution. Thereafter, the strips were again triturated in modified KB solution through a pipette (tip diameter 0.8–1.2 mm) for 5–10 min. Single cells obtained during this step were stored at room temperature in modified KB solution for at least 45 min. Samples of the cell suspension (0.4 ml) were placed in recording chambers on the stages of two inverted microscopes (Diaphot; Nikon Inc., Melville, NY). The cells were allowed to settle for 5–10 min, after which superfusion with normal Tyrode solution (0.6 ml/min) was started. For our coupling clamp experiments, we selected moderately sized spindle and elongated spindle-like cells (Denyer and Brown, 1987) that had not rounded up after readministration of calcium ions to the bathing solution and displayed regular spontaneous electrical activity. Electrophysiological recordings were performed at a temperature of 35 ± 0.5°C. The temperature of the bathing solution was monitored continuously with a thermistor probe and was maintained by a translucent heating plate underneath the bottom of the recording chamber.

### *Solutions*

Normal Tyrode solution contained (mM) 140 NaCl, 5.4 KCl, 1.8 $CaCl_2$, 1.0 $MgCl_2$, 5.0 HEPES, 5.5 glucose, pH adjusted to 7.4 with NaOH. The composition of nominally $Ca^{2+}$-free Tyrode solution was the same as of normal Tyrode solution, except the $CaCl_2$ was omitted. The enzyme solution contained collagenase B (0.28 U/ml; Boehringer-Mannheim, Mannheim, Germany), pronase E (0.92 U/ml; Serva, Heidelberg, Germany), elastase (12.4 U/ml; Serva), and bovine serum albumin (1 mg/ml), in nominally $Ca^{2+}$-free Tyrode solution. Modified KB solution contained (mM): 85 KCl, 30 $K_2HPO_4$, 5.0 $MgSO_4$, 20 glucose, 5.0 pyruvic acid, 5.0 creatine, 30 taurine, 0.5 EGTA, 5.0 β-hydroxybutyric acid, 5.0 succinic acid, 2.0 $Na_2ATP$, 50 g/liter polyvinylpyrrolidone, pH adjusted to 6.9 with KOH. The composition of the internal pipette solution was (mM) 125 K-gluconate, 20 KCl, 10

HEPES, pH adjusted to 7.1 with KOH. The external solution was normal Tyrode solution.

### *Electrophysiological Recording*

Simultaneous patch clamp recordings were made from two single isolated SA nodal myocytes, with the cells residing in two separate cell chambers in separate but essentially identical setups. Membrane potentials and currents were recorded using the amphotericin-perforated patch technique (Rae et al., 1991). With this technique, intracellular dialysis is prevented and the intracellular calcium concentration is allowed to change with time during the action potential. The recording period without significant changes in action potential shape of either cell of the cell pair was typically ~15 min. Changes were considered significant if maximum diastolic potential or action potential amplitude changed by >3 mV, or if interbeat interval changed by >10 ms. Pipettes were pulled from borosilicate glass and heat polished. The pipettes had resistances of 3–5 MΩ when filled with the internal pipette solution. Shortly before the experiment, 6 mg amphotericin B (Sigma Chemical Co., St. Louis, MO) was dissolved in 100 μl DMSO, of which 10 μl were added to 3 ml internal pipette solution. Pipette tips were immersed in normal internal pipette solution for 1 s, and subsequently backfilled with the pipette solution to which amphotericin was added. Within 10 min after sealing to the membrane, a series resistance of 8–12 MΩ was obtained that remained stable throughout the experiment. This series resistance was compensated up to ~90%. Apart from zeroing the potential before touching the cell surface by the pipette tip, no attempts were made to correct for junction potential. Recordings were made with custom-built dual amplifiers. Data were sampled directly into Macintosh Quadra 650 microcomputers (Apple Computer, Inc., Cupertino, CA) using custom-written data acquisition software, and stored on disk for off-line processing using custom-written data analysis software.

We defined the membrane capacitance for our cells as the amplitude of a small hyperpolarizing current pulse (typically 20–40 pA) of 100-ms duration, divided by the initial slope of the transmembrane voltage in response to this current pulse. The current pulse was adjusted to produce a membrane hyperpolarization of ~10 mV, and was switched on shortly after the action potential had reached its maximum diastolic potential. Input resistance was defined as the amplitude of the steady state voltage response divided by the current amplitude, and input conductance as the reciprocal value of input resistance. Membrane capacitance of the cells used in our coupling clamp experiments was 40 ± 3 pF (mean ± SD, $n = 10$). Input resistance was 0.46 ± 0.12 GΩ (mean ± SD, $n = 10$), which is in general agreement with those observed by others (Irisawa et al., 1987; Denyer and Brown, 1990).

### *Action Potential Parameters*

The action potentials of the SA nodal cells used in our coupling clamp experiments were characterized by seven action potential parameters. These parameters were determined from 5–10 consecutive action potentials using custom-written data analysis software and are listed in Table I. Maximum diastolic potential (MDP) is the most negative value of membrane potential. Action potential amplitude is the amplitude of the action potential, measured as the peak positive potential minus the maximum diastolic potential. Interbeat interval (IBI) is the time between 50% depolarization on one upstroke and 50% depolarization on the next. Action potential duration at 50% repolarization ($APD_{50}$) is the time between 50% depolarization and 50% repolarization of the action potential. Similarly, action potential duration at 90% repolarization ($APD_{90}$) is the time between 50% depolarization and 90% repolarization of the action potential. Diastolic depolarization rate (DDR) is $\Delta V_m/\Delta t$, where $\Delta V_m$ is the change in membrane potential ($V_m$) during a 75-ms time interval (i.e., $\Delta t = 75$ ms) starting at a membrane potential that is 1 mV positive to the MDP. Maximum upstroke velocity ($V_{max}$) is the maximum rate of change of the membrane potential (i.e., the maximum value of $dV_m/dt$) attained during the upstroke of the action potential.

### *Coupling Two Isolated Sinoatrial Nodal Cells Together*

The method used for electrical coupling of two isolated rabbit SA nodal cells is illustrated in Fig. 1. Fig. 1 *A* is a diagram of two cells, labeled 'cell A' and 'cell B,' which are electrically coupled by a coupling conductance ($G_c$; in siemens). If the membrane potentials (in volts) of the two cells are $V_{m,A}$ and $V_{m,B}$, both functions of time, then the coupling current ($I_c$; in amperes) flowing from cell A to cell B, also a function of time, would be continuously given by $I_c = G_c \times (V_{m,A} - V_{m,B})$. Thus, a current $I_c$ (positive or negative) is continuously leaving cell A and entering cell B. The computer (labeled 'PC') accomplishes this coupling by repetitively sampling, at a period of 130 μs, the membrane potentials of the two cells, computing the value of $I_c$, and then sending this value via a digital-to-analog (D/A) converter to each of the two voltage-to-current converters (labeled 'V→I'), as illustrated in Fig. 1 *B*. The value of $I_c$ is sent directly to the voltage-to-current converter associated with cell A and is sent as an inverted signal to the voltage-to-current converter associated with cell B. The computer can thus couple the cells with any desired value of $G_c$ and also rapidly turn this conductance on or off as a function of time. Note that the cell pairs studied always consisted of two cells being simultaneously studied in two separate microscope setups, thus precluding any electrical contact between the cells except that provided by the coupling circuit. Custom-written coupling clamp software was compiled as a DOS real mode application using Borland Pascal (version 7.0; Borland International, Scotts Valley, CA) and run on a 60-MHz Pentium processor computer equipped with a moderately fast 12-bit data acquisition board (model PCL-718; American Advantech, Sunnyvale, CA).

Since we measure the membrane capacitance ($C_m$; in farads) of each cell and we record the membrane potential as a function of time, we can compute the capacitative current ($I_{cap}$; in amperes) of each cell (as a function of time) as $C_{m,A}\, dV_{m,A}/dt$ and $C_{m,B}\, dV_{m,B}/dt$ for cells A and B, respectively. For each cell, it must be true that the sum of the ionic membrane currents entering or leaving the cell ($I_{ion}$), the coupling current, and the capacitative current must be zero at all times; i.e., $I_{ion} + I_c + I_{cap} = 0$. Therefore, we can compute the ionic membrane current of cells A and B as $I_{ion,A} = -C_{m,A}\, dV_{m,A}/dt - I_c$ and $I_{ion,B} = -C_{m,B}\, dV_{m,B}/dt + I_c$, respectively, as functions of time. This computation makes no assumptions concerning the actual ionic conductances of the cell membrane, with the computed $I_{ion}$ being the sum at each time step of the inward and outward ionic currents across the cell membrane.

In our standard protocol, coupling is switched on after a 2-s period of recording at zero coupling conductance. Coupling stays on for 6 s, and is then switched off, ending the 10-s run with another 2-s period of uncoupling (see Figs. 2–5, below). The membrane potential of cells A and B and the coupling current are displayed during the run, thus providing real-time information on the coupling process. The computer program stores as an array the successive samples of the membrane potentials of the two cells. At the end of the run, these samples are transferred to disk, together with parameter settings. With this information, a second program can then off-line "replay" the experimental protocol, producing a disk file with a time sequence of the membrane po-

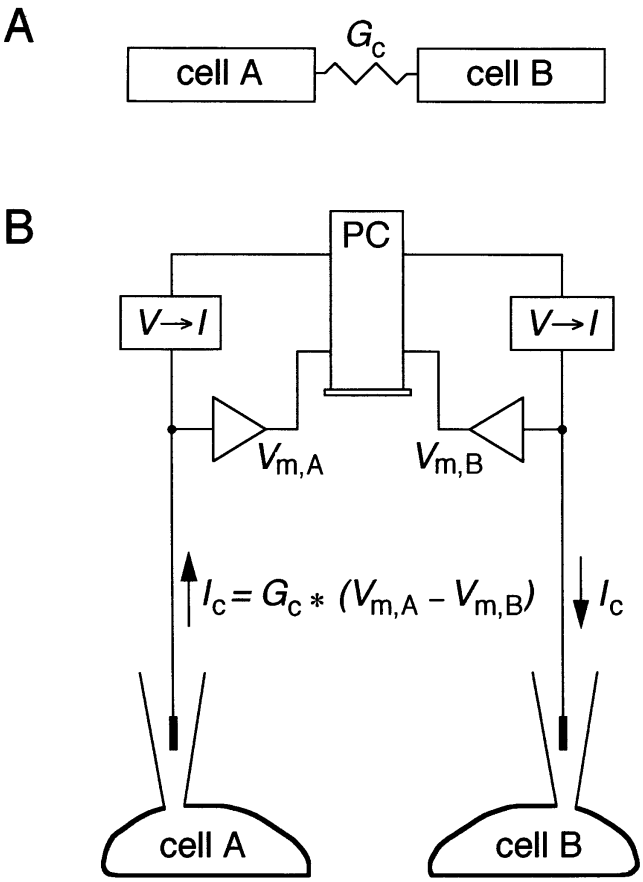


FIGURE 1. Diagram of the experimental system in which we electrically coupled two isolated sinoatrial node cells. (*A*) Overall experimental design in which our technique introduces a coupling conductance $G_c$ between two patch-clamped isolated cells (*cell A* and *cell B*). (*B*) Simultaneous patch clamp recordings for cells A and B in the "current clamp" mode produce membrane potentials $V_{m,A}$ and $V_{m,B}$, respectively, which are sampled by the computer (*PC*) via an A/D converter at each time step. The computer multiplies the difference in the two membrane potentials by a desired value of $G_c$, thus producing the equivalent $I_c$, which would have been present if the cells had indeed been electrically coupled. A voltage proportional to the desired $I_c$ is output from the computer via a D/A converter and through a voltage-to-current converter ($V \rightarrow I$) as $+I_c$ to cell A and through a separate set of converters as $-I_c$ to cell B.

tentials of the two cells, the coupling current, and any computed parameters of the cells (e.g., the capacitative currents and the membrane ionic currents) as functions of time.

It is likely that electrical interactions between SA nodal cells depend on cell size. As not all isolated SA nodal cells are similar in size, we have adopted a method of standardizing cell size before starting the coupling clamp experiments. We previously showed that major membrane ionic currents in isolated SA nodal cells are proportional to $C_m$ (Wilders et al., 1996). Therefore, we used $C_m$ to standardize cell size and set the effective "size" of either cell to 40 pF. The procedure we use is as follows. First, we online estimate $C_{m,A}$ and $C_{m,B}$ and compute size factors $z_A = C_{m,A}/40$ and $z_B = C_{m,B}/40$ for cell A and cell B, respectively. During the experiment, the current inputs for cell A ($I_c$) and for cell B ($-I_c$) are replaced with $I_c \times z_A$ and $-I_c \times z_B$, respectively. Thus, the current input for an 80-pF cell (size factor 2) is twice that for a 40-pF cell, so that an 80-pF cell interacts like a 40-pF cell. In all experiments, the on-line estimates of $C_{m,A}$ and $C_{m,B}$ were 40 pF. Consequently, size factors $z_A$ and $z_B$ amounted to 1 in all experiments. Later off-line analysis revealed that the true values of $C_m$ (listed in Table II) differed only slightly from their on-line estimates.

## RESULTS

### *Increasing Coupling Conductance*

Fig. 2 shows simultaneous recordings from two SA nodal cells, with the membrane potential recordings of the two cells distinguished by a solid (for cell A) or dotted (for cell B) line. Data for Fig. 2, as well as Figs. 3–7, are from experiment 950803-2 (Table II). Fig. 2 *A* (*top*) shows the experimental protocol in which the recordings were made without electrical coupling between the cells for two seconds, followed by a period of 6 s of electrical coupling at 0.10 nS, and then by a second period of uncoupling for 2 s. During the periods of uncoupling, the spontaneous activity of cell A is occurring at a shorter interbeat interval (310 ms) than the spontaneous activity of cell B (390 ms). The action potentials of the two cells are also somewhat different in shape, with cell A having a less negative maximum diastolic potential (−57 vs. −62 mV) and a less positive peak amplitude (26 vs. 28 mV) than cell B. Cell A also has a shorter action potential duration than cell B. The measured action potential parameters for these cells, when uncoupled, are listed in Table I, along with the parameter values for the cells of the other four cell pairs from which recordings were made. The Fig. 2 *A* (*bottom*) plots the coupling current for this cell pair. The coupling current is, of course, zero during the two periods of uncoupling, and is plotted as a positive current in the direction from cell A to cell B.

During the 6 s of coupling in Fig. 2 *A*, it is clear that the action potentials of cells A and B are not entrained to each other in a 1:1 manner. To aid in the interpretation, we have labeled the action potentials of cell A during the coupling period as sequential numbers 1–19. In addition, we have plotted in Fig. 2 *B* the data of the central time period of Fig. 2 *A* (as indicated by the horizontal two headed arrow) at a faster time base. Cell A action potential numbers 1–6 are occurring during the diastolic period of the action potentials of cell B and can be seen to be associated with the corresponding action potentials of cell B such that the delay between the action potentials of cell A and those of cell B is progressively increasing. Action potential number 7 of cell A produces a depolarization during the diastolic period of cell B and this depolarization actually delays the subsequent activation of cell B. The subsequent activation of cell B (indicated by the single vertical arrow head) occurs before action potential number 8 of cell A and

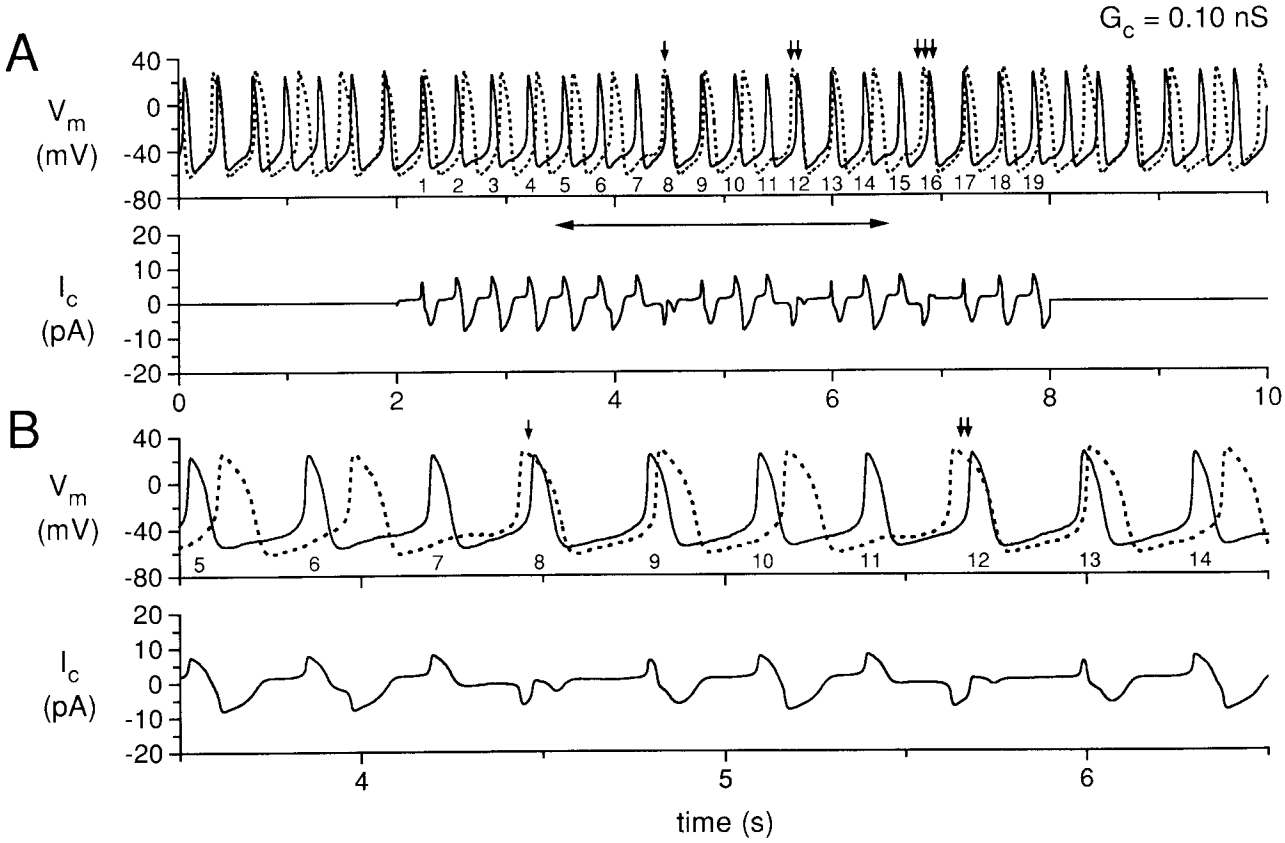


FIGURE 2. Simultaneous recording for 10 s of two isolated sinoatrial node cells, with the cells uncoupled during the first and last 2 s and coupled with a coupling conductance of 0.10 nS during the central 6 s. (*A*) Membrane potential ($V_m$) of cell A (*solid line*) and cell B (*dotted line*), and coupling current ($I_c$). The action potentials of cell A during the coupling period are numbered 1–19 for reference. The small vertical arrows indicate action potentials for which the action potential of cell B occurs before the corresponding action potential of cell A. (*B*) Data in *A* replotted for the time period indicated by the horizontal two headed arrow in *A*. Data from experiment 950803-2 (see Tables).

actually shortens the cycle length between action potentials 7 and 8 of cell A. Action potentials 9 and 10 of cell A, however, reestablish the previous condition of cell A activating before cell B, although with increasing time delay between the activation of cell A and the activation of cell B. Action potential number 11 of cell A, however, repeats the process observed for action potential 7 of cell A, with a failure to directly produce an ac-

TABLE I

*Action Potential Parameters of Rabbit Sinoatrial Node Cells Used in Coupling Clamp Experiments*

| Cell | MDP | APA | IBI | $APD_{50}$ | $APD_{90}$ | DDR | $\dot{V}_{max}$ |
|---|---|---|---|---|---|---|---|
| | *mV* | *mV* | *ms* | *ms* | *ms* | *mV/s* | *V/s* |
| 950111A | −56 | 82 | 358 | 118 | 148 | 136 | 4.3 |
| 950111B | −61 | 86 | 331 | 77 | 104 | 101 | 4.4 |
| 950117A | −56 | 84 | 236 | 79 | 105 | 145 | 6.4 |
| 950117B | −55 | 83 | 257 | 68 | 97 | 93 | 6.7 |
| 950131A | −45 | 66 | 344 | 75 | 106 | 59 | 2.9 |
| 950131B | −59 | 78 | 424 | 88 | 119 | 68 | 3.4 |
| 950803-1A | −61 | 90 | 279 | 64 | 81 | 117 | 9.3 |
| 950803-1B | −68 | 93 | 442 | 119 | 148 | 50 | 7.9 |
| 950803-2A | −57 | 83 | 310 | 60 | 81 | 95 | 7.0 |
| 950803-2B | −62 | 90 | 390 | 115 | 143 | 80 | 6.8 |
| Mean ± SD | −58 ± 6 | 84 ± 8 | 337 ± 69 | 86 ± 23 | 113 ± 26 | 94 ± 32 | 5.9 ± 2.1 |
| Model | −66 | 97 | 388 | 92 | 125 | 78 | 6.9 |

MDP, maximum diastolic potential; APA, action potential amplitude; $\dot{V}_{max}$, maximum upstroke velocity.

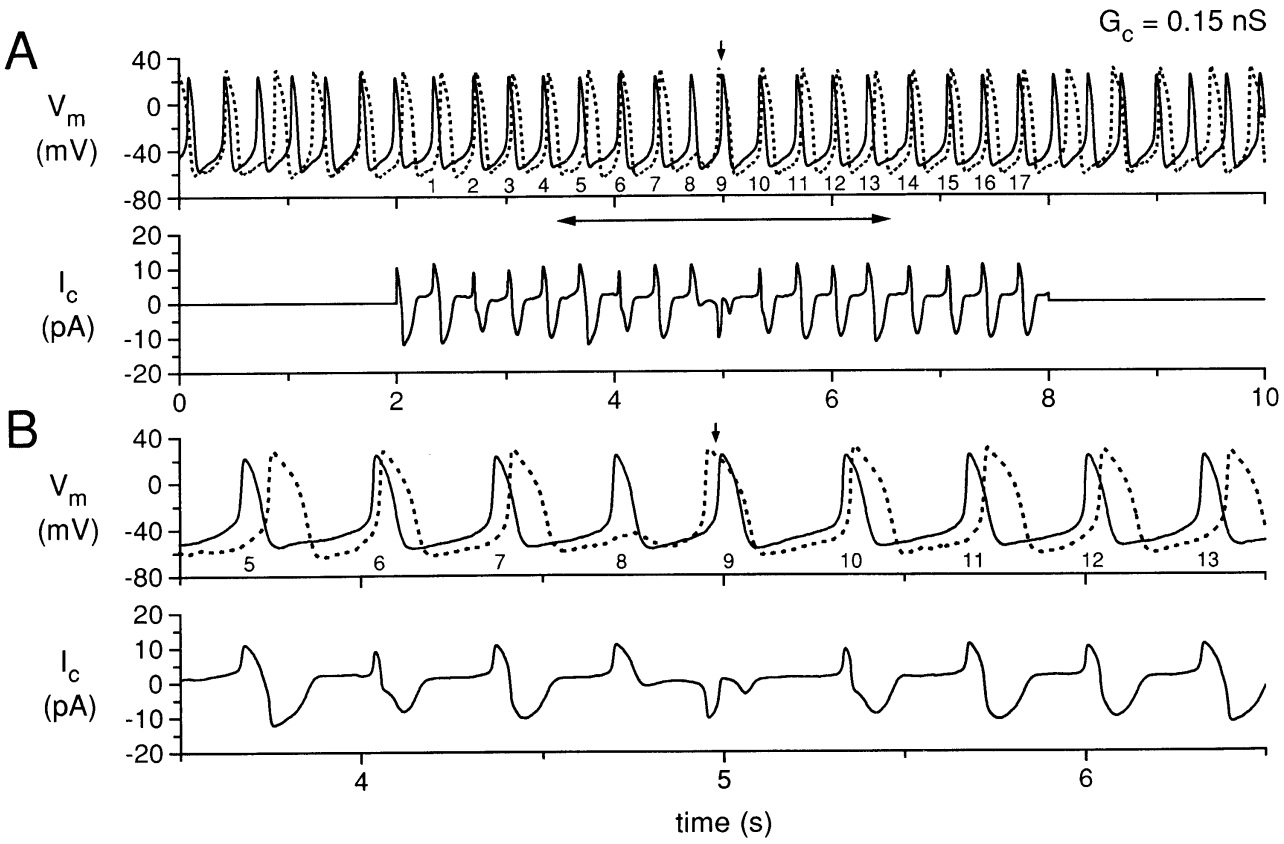


FIGURE 3. Simultaneous recording for 10 s of two isolated sinoatrial node cells, with the cells uncoupled during the first and last 2 s and coupled with a coupling conductance of 0.15 nS during the central 6 s. (*A*) Membrane potential ($V_m$) of cell A (*solid line*) and cell B (*dotted line*), and coupling current ($I_c$). The action potentials of cell A during the coupling period are numbered 1–17 for reference. The small vertical arrow indicates an action potential for which the action potential of cell B occurs before the corresponding action potential of cell A. (*B*) Data in *A* replotted for the time period indicated by the horizontal two headed arrow in *A*. Data from experiment 950803-2 (see Tables).

tion potential in cell B, a delayed cycle length for cell B, or a reversal of the sequence of activation (cell B before cell A) for action potential number 12 of cell A (Fig. 2 *A, vertical arrow head*). This process then repeats again for action potentials numbered 15 and 16 of cell A, as indicated by the triple vertical arrow head. The lower panels of Fig. 2, *A* and *B*, show the simultaneously occurring coupling current.

Figs. 3–5 show data from the same cell pair in the same presentation format as for Fig. 2, using values of coupling conductance of 0.15 nS (Fig. 3), 0.20 nS (Fig. 4), and 10 nS (Fig. 5). For the period of coupling illustrated in Fig. 3, each of the action potentials (numbered 1–17) for cell A occur before an associated action potential of cell B, except action potentials numbered 8 and 9. For these two action potentials, the process described for Fig. 2 occurs, in which action potential number 8 of cell A produces a subthreshold depolarization during the diastolic period of cell B and this depolarization in cell B delays the subsequent activation of cell B. This subsequent activation of cell B occurs before action potential number 9 of cell A (Fig. 3 *A, arrow*), but action potential number 10 of cell A reestablishes the pattern of the action potential of cell A occurring before the associated action potential of cell B. Note that, at this higher value of coupling conductance (0.15 nS), this process occurs only once during the coupling period, as compared with the three occurrences during the coupling period when the coupling conductance was 0.1 nS (Fig. 2).

In Fig. 4 ($G_c$ = 0.2 nS), a stable pattern of entrainment of the action potentials of cells A and B is established during the period of coupling. Note that the coupling current increases in magnitude from Fig. 2 to Fig. 3 to Fig. 4 as the coupling conductance increases. In Fig. 4, the action potentials of cells A and B are entrained at a common interbeat interval, but the shapes of the action potentials are still quite different for cell A and cell B, with cell B retaining a more negative maximum diastolic potential and a longer action potential duration. In other words, the cells show "frequency entrainment," but not "waveform entrainment" (Cai et

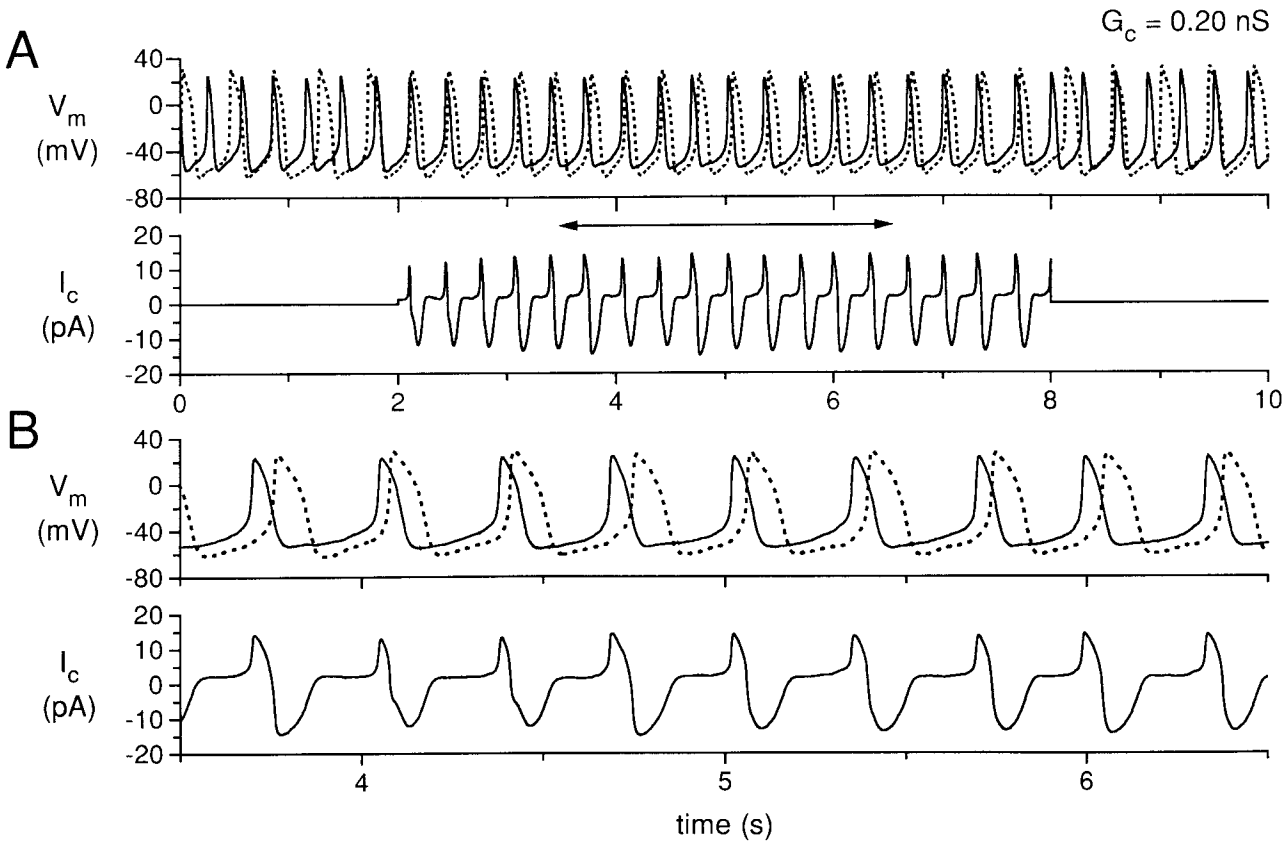


FIGURE 4. Simultaneous recording for 10 s of two isolated sinoatrial node cells, with the cells uncoupled during the first and last 2 s and coupled with a coupling conductance of 0.20 nS during the central 6 s. (*A*) Membrane potential ($V_m$) of cell A (*solid line*) and cell B (*dotted line*), and coupling current ($I_c$). (*B*) Data in *A* replotted for the time period indicated by the horizontal two headed arrow in *A*. Data from experiment 950803-2 (see Tables).

al., 1994). When the coupling conductance is further increased to 10 nS (Fig. 5), the action potentials of cells A and B are nearly synchronous during the period of coupling, with the action potential shapes now also nearly identical: the cells show both frequency and waveform entrainment. The coupling current is further increased in magnitude, although now the positive peak of the coupling current (from cell A to cell B) is much sharper during each cycle as the upstrokes of the two cells are synchronized. As before, there is a significant negative component of coupling current (flowing from cell B to cell A) due to the intrinsically longer APD of cell B. During diastolic depolarization, a sustained "tonic" component of coupling current, amounting to ~10 pA, is flowing from cell A to cell B.

*Activation Delay*

If we define the successive activation times of either cell A or cell B as the times at which the membrane potential crosses zero in a positive direction, we can analyze the effects of the coupling conductance on the time-varying interbeat intervals and the activation delays between cells A and B for coupled action potentials. Fig. 6 illustrates the effects of coupling conductance of either 0.1 (part A) or 0.15 (part B) nS for the same cell pair used for Figs. 2–5. In Fig. 6 *A*, the IBI of the two cells fluctuates over a range of ~25 ms during the initial period of uncoupling of the first 2 s. The horizontal arrow (Fig. 6 *A*) indicates the time period of coupling. Immediately after the coupling was established, there is a tendency of the IBI values of the two cells (cell A, ●; cell B, □) to become nearly the same, but this tendency is interrupted by the interactions described in Fig. 2, with three occurrences of long IBI for cell B in a cyclical pattern. Note that the presence of a low value of coupling conductance (0.1 nS) actually increases the variability over time of the IBI for both cells A and B as compared with the fluctuations during the uncoupled periods. We plotted the activation delay (▲) between cell A and cell B only for the time period of coupling in the lower panel of Fig. 6 *A*. Since cell A has an intrinsically shorter IBI than cell B, we use the times of occurrence of activation of cell A as the index times for the determination of activation delay from cell A to cell B. There are three discontinuities in the plot of activation delay

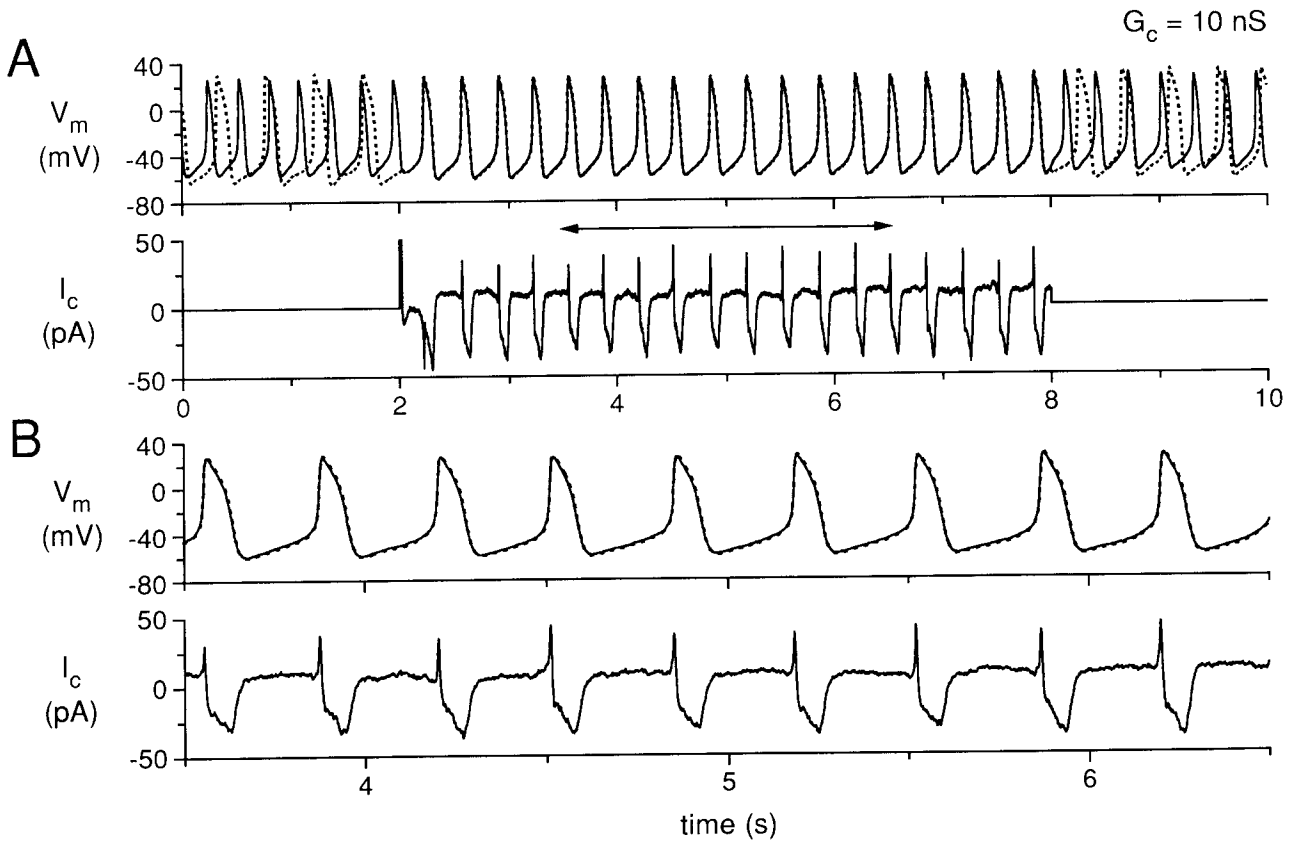


FIGURE 5. Simultaneous recording for 10 s of two isolated sinoatrial node cells, with the cells uncoupled during the first and last 2 s and coupled with a coupling conductance of 10 nS during the central 6 s. (*A*) Membrane potential ($V_m$) of cell A (*solid line*) and cell B (*dotted line*), and coupling current ($I_c$). (*B*) Data in *A* replotted for the time period indicated by the horizontal two headed arrow in *A*. Data from experiment 950803-2 (see Tables).

associated with action potentials of cell A, which were labeled as 7, 11, and 15 in the plot of Fig. 2 for this cell. For these action potentials, the associated response of cell B is a subthreshold depolarization and the subsequent action potentials in cell B clearly arise before the next action potentials in cell A. Therefore, the actual activation delay is negative (with respect to the activation times of cell A) for action potentials 8, 12, and 16 of cell A. For Fig. 6 *B*, we plot the IBI and the activation delay for the data (from the same cell pair) plotted in Fig. 3 for a higher value of coupling conductance (0.15 nS). Compared with the results of Fig. 6 *A* with the lower value of coupling conductance (0.1 nS), there is now more of a tendency for the IBI of the two cells to achieve a common value during the coupling period, with a predominant shortening of the IBI of the faster cell. However, there is a singular occurrence of the same process that occurred three times for Fig. 6 *A*, with a long IBI for the slower cell at a time of 5 s. This process also causes an apparent reversal in the direction of the activation for the beat after the long cycle length, thus producing a single negative value of activation delay.

Fig. 7 shows the IBI and the activation delay for the two higher values of coupling conductance for which the action potentials of cells A and B were entrained at a common IBI during the coupling period. For Fig. 7 *A* (coupling conductance, 0.2 nS), the two cells again show fluctuations of their IBI during the uncoupled periods, but during the coupling period the IBI of the two cells has a mean value slightly larger than that of the uncoupled IBI of cell A. Note that the common IBI is clearly not the arithmetic average of the IBI values for each of the cells. Fluctuations of IBI still occur during the coupling period with differences of up to 34 ms for IBI values of the two cells even for cycles that are associated in time as part of the entrainment process. The activation delay (Fig. 7 *A, bottom*) shows significant fluctuations from 24 to 64 ms with an average value of 43 ms. For Fig. 7 *B* (coupling conductance, 10 nS), the two cells have a common IBI during the coupling period that still varies somewhat with time, but for each cycle the IBI values for the two cells are nearly equal. The activation delay is now $<1$ ms for each cycle and shows very little fluctuation during the coupling period. For the first coupled action potential, cell B fires before cell

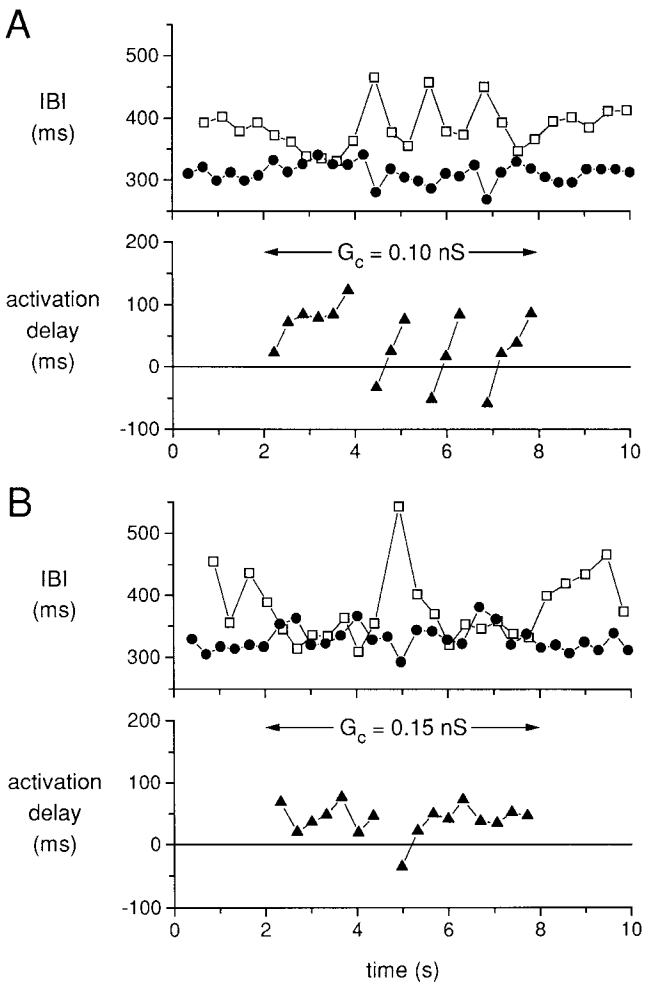


FIGURE 6. Interbeat interval (*IBI*) for cells A and B (*top*, ● and □, respectively) and the delay in activation of cell B with respect to the activation of cell A (*bottom*, ▲) for a coupling conductance $G_c$ (*horizontal arrow*). (*A*) $G_c$ = 0.10 nS. (*B*) $G_c$ = 0.15 nS. The data in *A* and *B* come from the action potential recordings of Figs. 2 and 3, respectively. Data from experiment 950803-2 (see Tables).

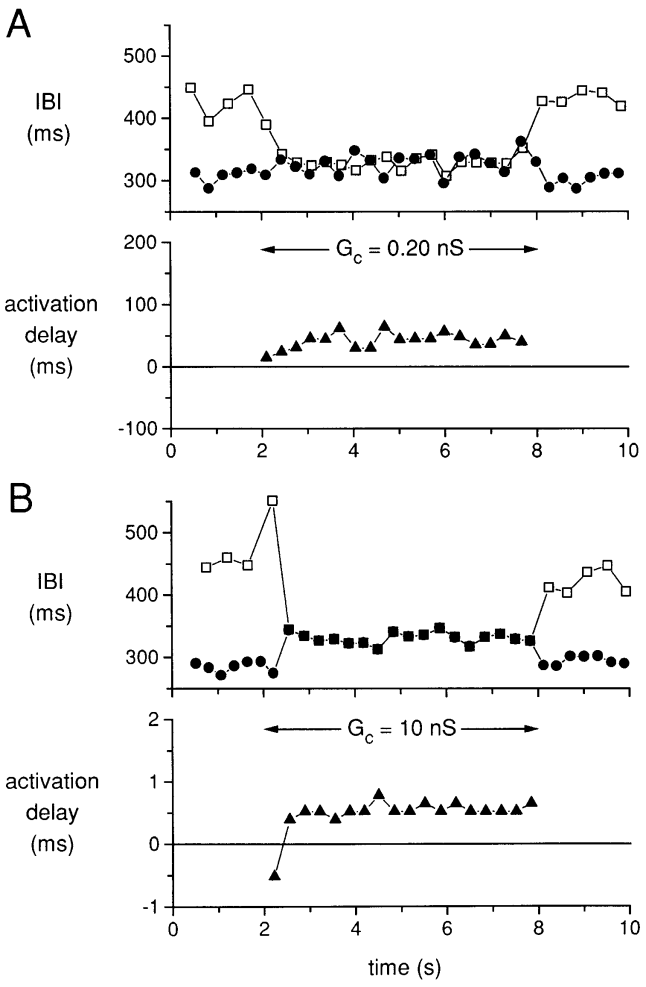


FIGURE 7. Interbeat interval (*IBI*) for cells A and B (*top*, ● and □, respectively) and the delay in activation of cell B with respect to the activation of cell A (*bottom*, ▲) for a coupling conductance $G_c$ (*horizontal arrow*). (*A*) $G_c$ = 0.2 nS. (*B*) $G_c$ = 10 nS. The data in *A* and *B* come from the action potential recordings of Figs. 4 and 5, respectively. Data from experiment 950803-2 (see Tables).

A, resulting in a negative activation delay and a negative spike in coupling current at 2.2 s (Fig. 5 *A, bottom*).

*Membrane Ionic Current*

The presence of a high value of coupling conductance (10 nS) between cell A and cell B not only makes the action potential shapes and IBI of the two cells the same, but also produces very significant changes in the membrane ionic currents of the two cells. In Fig. 8, we have superimposed action potentials recorded from cell A and cell B at zero coupling conductance. The solid and dotted action potentials of cells A and B, respectively, have been aligned in time such that the upstrokes of the first action potential of each cell are simultaneous, with the zero time adjusted for each trace. The cycle length for cell A is shorter than the cycle length of cell B, producing a nonsynchronous occurrence of the second action potential for each cell, with the second action potential for cell A occurring before the second action potential of cell B. When we examine the total membrane ionic currents of the two cells ($I_{ion,A}$ as a solid line and $I_{ion,B}$ as a dotted line) shown in Fig. 8 *B*, with each ionic current trace aligned with the corresponding action potential trace for each cell, we see that the membrane ionic current of each cell is negative (inward) during the diastolic period of each cell action potential as expected, with comparable values of −3 to −4 pA. The large inward current during the upstroke of each action potential is truncated at the gain used for the plot. During the early repolarization phase of each action potential, the membrane current of each cell is outward, with a larger outward current for cell A than cell B due to the more "plateau"-like repolarization of the action potential of cell B. During the

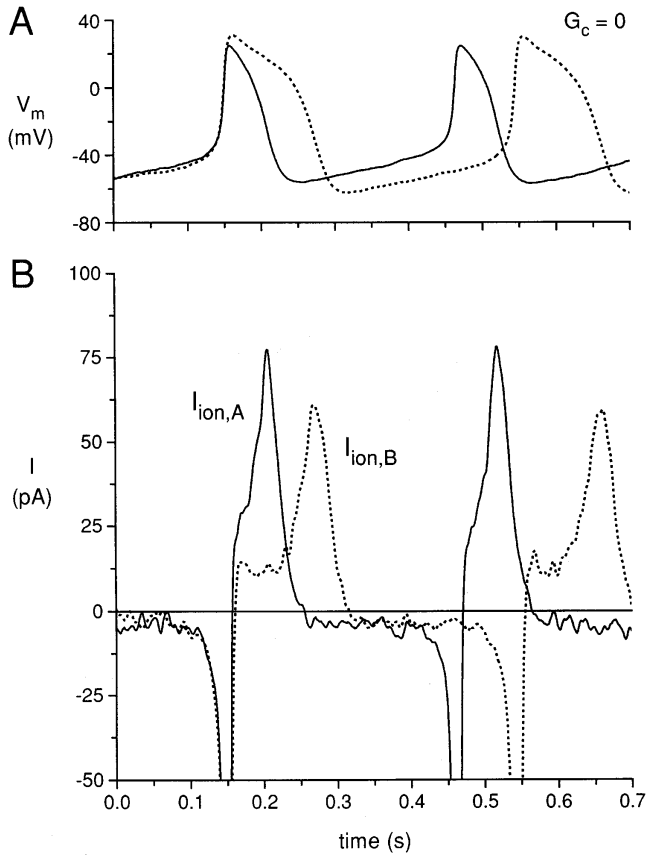


FIGURE 8. (*A*) Superimposed action potentials for the same cell pair used for Figs. 2–7 at zero coupling conductance, with the upstrokes of the first action potentials shown for each cell superimposed in time. (*B*) Calculated ionic membrane currents of cell A ($I_{ion,A}$; *solid line*) and cell B ($I_{ion,B}$; *dotted line*).

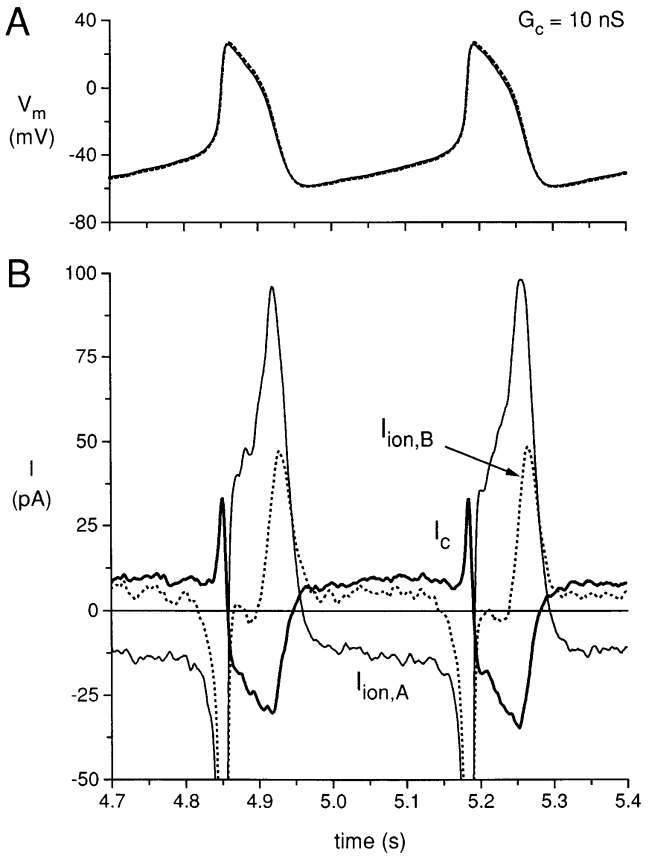


FIGURE 9. (*A*) Simultaneously recorded action potentials from the coupled period for the same cell pair used for Figs. 2–7 at a coupling conductance of 10 nS. (*B*) Calculated ionic membrane currents of cell A ($I_{ion,A}$; *solid line*) and cell B ($I_{ion,B}$; *dotted line*), and the coupling current ($I_c$; *bold solid line*).

final repolarization phase of each action potential, the current is large and positive for both cells A and B, with a peak outward current of 77 pA for cell A and 60 pA for cell B.

In Fig. 9, we plot the action potentials of the same cell pair for the time period of coupling at 10 nS from 4.7 to 5.4 s of Fig. 5. For part A, the action potentials are now synchronous in occurrence and with nearly identical shapes. The corresponding membrane ionic currents and the coupling current are plotted in part B, with the coupling current ($I_c$) plotted as a bold solid line. During the diastolic depolarization phase, the membrane current of cell A is now much more negative than the current for the diastolic depolarization for the same cell when uncoupled (see Fig. 8), even though the diastolic depolarization phase of cell A is prolonged by the presence of the coupling conductance. The membrane current of cell B is now actually positive during the diastolic depolarization phase of cell B, which seems somewhat paradoxical since the membrane potential of cell B is steadily depolarizing during this phase. Note that the coupling current is positive (in the direction from cell A to cell B) during the synchronized diastolic depolarization phases of the two cells. The presence of this coupling current of ~9 pA, being a transfer of charge from cell A to cell B, induces a larger inward membrane ionic current (~−13 pA) in cell A and an actual positive current (~6 pA) in cell B, such that the capacitative currents of both cell A and cell B amount to −3 to −4 pA, corresponding with a diastolic depolarization rate of ~80–90 mV/s.

The presence of electrical coupling also affects the membrane ionic currents during the repolarization phases of the action potentials. The coupled action potential has an early repolarization phase that is slower than the uncoupled early repolarization phase of cell A and faster than the uncoupled early repolarization phase of cell B. During this phase, the coupling current is negative (from cell B to cell A) and this induces a larger outward current in cell A than the value present when cell A was uncoupled and induces a smaller outward current in cell B (nearly zero) as compared with the value when cell B was uncoupled. Also, the peak outward ionic membrane currents for cells A and B,

when coupled, are quite different than when uncoupled. The peak outward current for cell A increased from 77 to 97 pA and the peak outward current for cell B decreased from 60 to 48 pA.

*Common Interbeat Interval*

For the five cell pairs for which the basic data are summarized in Table II, there was a considerable intrinsic variability in the IBI of each cell when uncoupled. For two of the cell pairs, the IBI of the slower cell of the pair was within 10% of the IBI of the faster cell, while for one cell pair the IBI of the slower cell of the pair was ~60% longer than that of the faster cell. The other two cell pairs had intermediate values of difference for the IBI of the faster and slower cell of the cell pair. Since each of the cell pairs had a common IBI at a coupling conductance of 10 nS (frequency and waveform entrainment), this intrinsic difference in IBI of the cells of the cell pairs gave us an opportunity to determine how the intrinsic difference in the IBI determined the common IBI when well coupled. Fig. 10 *A* plots, for each of the cell pairs, the common IBI (expressed as a percentage of the intrinsic IBI of the faster cell, $IBI_f$), as a function of the intrinsic IBI of the slower cell ($IBI_s$, also expressed as a percentage of the $IBI_f$). If the common IBI were actually the average value of $IBI_f$ and $IBI_s$, then all of the points would fall along the dotted line of the figure, which is plotted with a slope of 0.5. It is clear that the points for which the $IBI_s$ of the cell pair was significantly greater than the $IBI_f$ of the cell pair deviate significantly from this relationship, with a clear tendency for the common IBI to be closer to the $IBI_f$ than to the $IBI_s$. This phenomenon was also observed in our recent publication (Wilders et al., 1996) in which we coupled two 40-pF model cells (using the Wilders-Jongsma-van Ginneken model of an isolated SA nodal cell; Wilders et al., 1991) together. In these model cell pairs, we systematically altered the maximum conductance for the hyperpolarizing activated current ($I_f$ current) of one of the cells to make the intrinsic IBI of one of the cells to be shorter or longer than the standard IBI of the cell model (388 ms), and then determined the common IBI of the two model cells when the two model cells were coupled by 10 nS. The simulation results are shown in the open circles of Fig. 10 *A* and agree very closely with the phenomenon observed for coupling of two real SA nodal cells.

*Critical Coupling Conductance*

We also determined, for the simulation study of two model SA nodal cells (Wilders et al., 1996), the critical value of coupling conductance above which the two model cells had the same IBI (frequency entrainment) and the simulation results from our previous work are plotted in Fig. 10 *B*, ○ with the critical coupling conductance as the ordinate and the IBI of the slower beating cell as the abscissa as for part A. We determined the critical coupling conductance for three of the cell pairs of the current study. For each cell pair, we have plotted the critical coupling conductance as a vertical range specified by the highest value of coupling conductance tested for which the cells were not frequency entrained (lower bound) and the lowest value of coupling conductance tested for which the cells were frequency entrained (upper bound). The three ranges of critical coupling conductance determined from the pairs of cells fall generally within the relationship determined from the simulation study. For the remaining two cell pairs, determination of the critical coupling conductance could not be completed before the action potential configuration of one of the cells became unstable. At the lowest value of coupling conductance tested (0.5 nS), these two cell pairs showed 1:1 frequency entrainment. So, for these two cell pairs, we can only state that the critical value of coupling conductance is ≤0.5 nS (Table II).

*Diastolic Depolarization Time*

To understand why the common IBI, when well coupled, for two cells that have intrinsically different values of IBI when uncoupled, is not simply the arithmetic average of the intrinsic IBI values, we have analyzed the

TABLE II

*Critical Coupling Conductance and Common Interbeat Interval of Rabbit Sinoatrial Node Cells. Coupling Clamp Data*

| Experiment | Membrane capacitance | | Input resistance | | Intrinsic interbeat internal | | Critical coupling conductance | Common interbeat interval* |
|---|---|---|---|---|---|---|---|---|
| | Cell A | Cell B | Cell A | Cell B | Cell A | Cell B | | |
| | *pF* | | *MΩ* | | *ms* | | *nS* | *ms* |
| 950111 | 44 | 36 | 420 | 650 | 358 | 331 | ≤0.50 | 342 |
| 950117 | 37 | 45 | 250 | 480 | 236 | 257 | 0.125–0.15 | 245 |
| 950131 | 40 | 39 | 300 | 460 | 344 | 424 | 0.20–0.30 | 375 |
| 950803-1 | 41 | 40 | 525 | 500 | 279 | 442 | ≤0.50 | 310 |
| 950803-2 | 41 | 39 | 520 | 510 | 310 | 390 | 0.15–0.17 | 333 |

*At a coupling conductance of 10 nS.

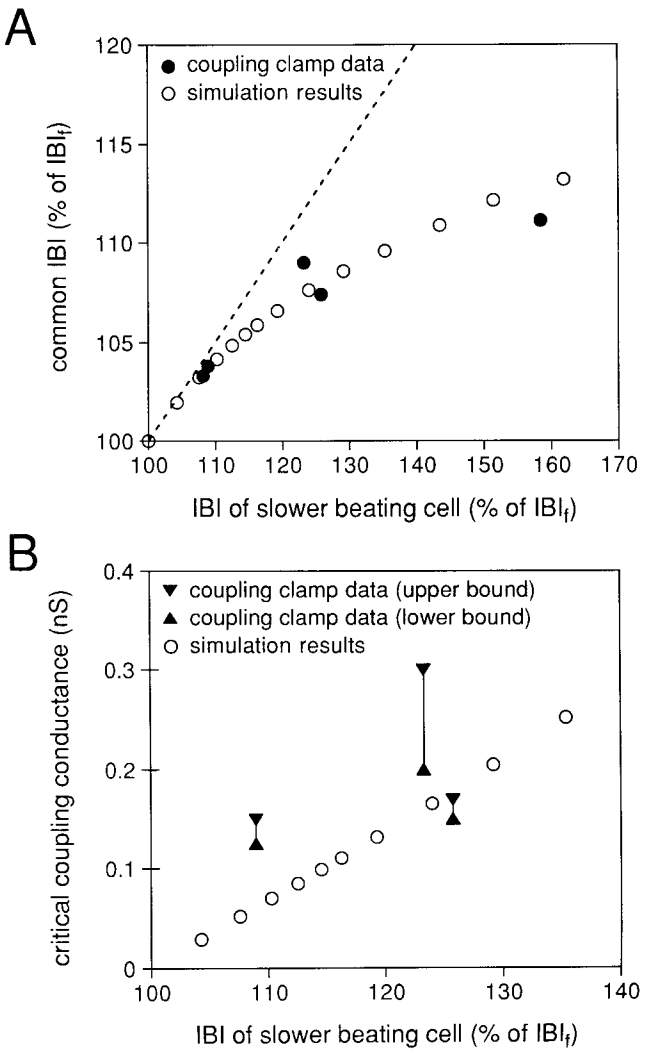


FIGURE 10. (*A*) Common interbeat interval (*IBI*) at a coupling conductance of 10 nS plotted (as a percentage of the IBI of the intrinsically faster beating cell, $IBI_f$) versus the IBI of the slower beating cell of the cell pair (also as a percentage of the $IBI_f$). Experimental results for the five cell pairs studied (●) and results obtained from a simulation of two pacing cells under the same conditions (○; see text). (*B*) Critical coupling conductance plotted versus the IBI of the slower beating cell of the cell pair (as a percentage of the $IBI_f$). Ranges experimentally obtained for three cell pairs (*solid symbols* and *lines*) and results obtained from a simulation of two pacing cells under the same conditions (○; see text). Note the difference in abscissa scales between *A* and *B*.

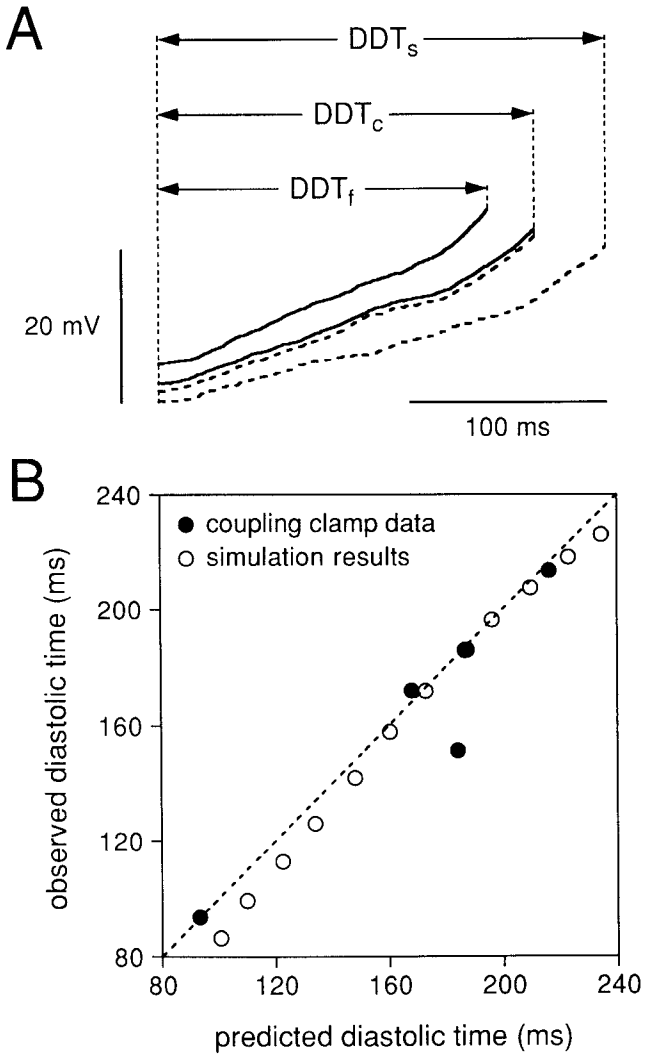


FIGURE 11. (*A*) Diastolic depolarization phase for the same cell pair used for Figs. 2–9 either when the two cells were uncoupled or when the cells were coupled by 10 nS. The diastolic intervals (DDT) are from the slower cell of the cell pair when uncoupled ($DDT_s$), the faster cell of the cell pair when uncoupled ($DDT_f$), and the simultaneously recorded diastolic intervals of the two cells when coupled ($DDT_c$). (*B*) Observed values of $DDT_c$ versus the values predicted from the uncoupled values of $DDT_s$ and $DDT_f$ using Eq. 3. The solid symbols show results for the five cell pairs studied, while the open symbols show results obtained from a simulation of two pacing cells under the same conditions (see text).

diastolic process of the cell pairs during conditions of complete uncoupling and with a coupling conductance of 10 nS. To quantitate the diastolic trajectory for each cell, we define a diastolic depolarization time (DDT) as the time required for the potential to rise from the maximum diastolic potential to a value 20 mV positive to this potential (Fig. 11 *A*). We chose a value of 20 mV as an approximation of the threshold potential with respect to the maximum diastolic potential, since for these spontaneously beating cells the exact value of voltage threshold cannot be defined. For each cell pair, we compute the DDT for the intrinsic uncoupled beating of the slower cell ($DDT_s$), for the intrinsic uncoupled beating of the faster cell ($DDT_f$), and for the coupled, synchronized beating of the cell pair with 10 nS of coupling conductance ($DDT_c$). Thus, the DDR for each cell would be:

$$DDR = \Delta V/DDT, \quad (1)$$

where $\Delta V = 20$ mV, and we can similarly define $DDR_s$,

$DDR_f$, and $DDR_c$. Since the DDR is determined by the capacitative current ($I_{cap} = C_m\, dV_m/dt$) and this capacitative current is equal to $I_{ion} + I_c$, but of opposite sign, the DDR for each cell is affected by the coupling current. As we showed in Fig. 5, there is a net coupling current during diastole for two coupled cells, which is in the direction from the cell that had the higher intrinsic DDR to the cell that had the lower intrinsic DDR. Since the magnitude of the coupling current is the same for the two cells (just being opposite in sign), we proposed the hypothesis that the change in DDR that occurred with coupling would be predicted as:

$$DDR_c = (DDR_s + DDR_f)/2. \quad (2)$$

In other words, the decrease in depolarization rate of cell A induced by the coupling current leaving cell A is equal to the increase in depolarization rate of cell B induced by the coupling current entering cell B. This hypothesis then predicts that the observed $DDT_c$ would be:

$$DDT_c = 2 \times (DDT_f \times DDT_s)/(DDT_f + DDT_s), \quad (3)$$

which follows from Eqs. 1 and 2. We measured $DDT_f$, $DDT_s$, and $DDT_c$ from each of the five cell pairs studied by using the averaged values of 10 successive action potentials during the coupled and uncoupled periods. Fig. 11 *A* shows the superimposed diastolic intervals of the same cells used for Figs. 2–7 with the corresponding DDT values indicated by horizontal arrows. Figs. 9 and 11 show the results of this analysis for all five cell pairs for which we plot the observed diastolic time when coupled versus the value of $DDT_c$ for each cell pair that was predicted from the observed $DDT_f$ and $DDT_s$. The dashed line has a slope of unity and corresponds to an exact agreement between the observed and predicted $DDT_c$. The experimental data points are shown as the filled symbols. The open symbols were produced by applying the same analysis to our simulation model in which two model SA nodal cells were coupled by 10 nS. There is a very good agreement with this simple analytical formulation both for the simulated pair of cells and for our experimental data from the five cell pairs.

## DISCUSSION

### *Coupling Clamp*

In this study, the dynamic electrical interactions between two pacemaker cells that underlie pacemaker synchronization in the SA node were studied. We investigated the required coupling conductance for synchronization and the electrical behavior of the SA nodal cells when coupled at levels of coupling conductance above and below that for which 1:1 entrainment occurs. To this end, the digital coupling clamp technique (Wilders et al., 1996) was used, which allows us to set any desired coupling conductance and effective cell size. This two-cell system uniquely enabled us to study electrical interactions without the complexity of a multidimensional syncytium. It is clear that the intact SA node will not behave as a single cell. The rabbit SA node consists of small clusters of pacemaker cells embedded in a considerable amount of connective tissue (de Maziére et al., 1992). These cell clusters are not strongly coupled to each other. In this context, the extension of our experimental protocol is simply a matter of scaling. To the extent that one can regard all of the cells within a given cluster of, for instance, 100 cells as isopotential, the cluster simply acts as a single cell with a size 100 times that of one cell. This does not mean that all cells need to be absolutely isopotential on a very short time scale. However, a limitation of this analogy is that in the SA node two cell clusters are likely to be connected to other cell clusters in a complex spatial pattern and our present experimental model is limited to the considerations of a single coupled cell pair of cells (or cluster of cells). Nevertheless, we feel that it is useful to consider a simpler system in which factors such as coupling conductance and effective cell size can systematically be varied.

However, there are some additional limitations in the applicability of the coupling technique we used. It appears extremely difficult to perform simultaneous current clamp measurements on two isolated nodal cells. Determination of the critical coupling conductance required measurements of ~20 min in which the action potential configuration of both cells of the cell pair had to remain stable. As a consequence, the success rate of this type of experiment is rather low.

In the present experiments, we assume that the coupling conductance can be treated as a constant value, independent of the membrane potential of either cell. It has been shown, however, that cardiac gap junctions do not always behave like pure ohmic resistors but can also exhibit time- and voltage-dependent kinetics (Rook et al., 1988; Anumonwo et al., 1992). In principle, we could adapt the technique to incorporate these kinetics. However, in rabbit SA nodal cell pairs, the time and voltage dependence is only observed if transjunctional voltage clamp steps of large amplitude and long duration are applied (Anumonwo et al., 1992). Furthermore, in a model study we have demonstrated that the stochastic open-close kinetics of the gap junctional channels hardly affect the process of synchronization of SA node cells (Wilders, 1993). Therefore, we considered the coupling conductance to be an ohmic resistor. It has also been shown that junctional conductance can be modulated by the intracellular calcium and magnesium levels and intracellular pH (Noma and Tsuboi, 1987; Spray and Burt, 1990). At this moment, no data is

available to show that these levels change during the time course of a single action potential. Therefore, we did not attempt to incorporate the dependence of coupling conductance on these levels. Another limitation of the coupling clamp technique is that the cells are not only electrically coupled, but also serve as pathways through which exchange of intracellular messengers occur.

### *Mutual Entrainment*

Sinoatrial node pacemaker cells behave as a population of electrically coupled oscillators, and their coordinated rhythm depends on the process of mutual entrainment (Winfree, 1967; Ypey et al., 1980). Mutual entrainment can be defined as a stable condition of electrical coupling between pacemaker cells with the result that the pacemaker cells have the same frequency (1:1 entrainment), or that their frequencies are harmonically related, but not necessarily with simultaneous discharges (Winfree, 1967). Since each cell would have a phasic influence on the other, it has been hypothesized that phase–response curves for each cell may give insight into their mutual interactions (Michaels et al., 1990; Ypey et al., 1982). It is assumed that the action potential of one cell acts as a depolarizing current pulse on the other cell and vice versa. By this mutual interaction, the two pacemakers would synchronize to a common IBI. Although the pacemakers fire with the same rhythm, they do not necessarily fire simultaneously. For the process of mutual entrainment to occur, there must always be some phase difference between them.

The process of mutual entrainment of rabbit SA node cells has been studied in SA node strips that were placed in a three-compartment tissue bath in which the central region was perfused with an ion-free sucrose solution permitting electrical insulation of the external segments (Jalife, 1984). In this "sucrose gap" study, it was shown that the dynamic interactions between two pacemakers resulted in mutual entrainment with both pacemakers beating at simple harmonic or complex ratios depending on the amount of coupling and the intrinsic interbeat intervals of the individual pacemakers.

In another study (Sano et al., 1978), the isolated SA node was partly divided into two parts by a cut in the middle portion. It was demonstrated that subthreshold depolarizing current pulses, when applied in the early portion of diastolic depolarization, prolong diastole, and when applied in the later portion, shorten it. Anumonwo et al. (1991) studied the phase resetting properties of single isolated SA node cells in response to brief current pulses and explained the mutual entrainment of SA node cells in terms of phase resetting. Theoretical studies explained the process of entrainment and synchronization of two (groups of) pacemaker cells (Cai et al., 1994; Ypey et al., 1980) and two-dimensional arrays of pacemaker cells (Cai et al., 1994), also in terms of phase–response curves. Analysis of phase–response curves based on an SA node model have shown that a phase delay produced by a brief depolarizing current pulse within the first half of the intrinsic IBI was due to a transient decrease in the slow inward current and the fast sodium current, while phase advances produced by brief depolarizing current pulses within the second half of its intrinsic period were due to a transient increase in the same currents (Michaels et al., 1986).

Although interactions between pacemaker cells are actually continuous rather than pulse-wise, these studies have provided insight into phase resetting interactions between pacemaker cells. In the present study, we have observed that phase resetting indeed occurs between two isolated SA node pacemaker cells when they are electrically coupled. In Fig. 2 *B* and the accompanying Fig. 6 *A*, it was shown that, at coupling conductances below the critical value for 1:1 entrainment, action potential 7 of cell A (the intrinsically faster beating cell) produces a small depolarization during the early diastolic phase of cell B. The consequence of this "subthreshold" depolarization was to delay the activation of cell B. This phase resetting effect clearly demonstrates its importance in the process of mutual entrainment in pacemaker cells.

In the present study, we demonstrate the existence of a recurrent phenomenon that was present at levels of coupling conductance below that required for 1:1 entrainment. This phenomenon consisted of a progressive increase in the activation delay between the cell with a shorter intrinsic IBI and the cell with an intrinsically longer IBI that was interrupted by a single activation failure, which then resets this process. As the coupling conductance was progressively increased toward the critical value for 1:1 entrainment, the frequency of occurrence of this phenomenon was decreased. This phenomenon may be related to Wenckebach periodicity of conduction through the atrioventricular node (AV node), although the situation we are creating consists of two coupled cells, both of which are intrinsically automatic and thus, when conduction failure does occur, the distal cell is still able to display a spontaneously generated activation.

### *Common Interbeat Interval*

One of the major determinants of the rate at which pacemaker cells fire their action potentials is the slope of diastolic depolarization. It is therefore generally assumed that the rhythm and frequency of the normal heartbeat is directed by the frequency of the SA node cell group with the steepest slope of diastolic depolar-

ization (Bleeker et al., 1980). For synchronization to occur, the most important requirement is that the mechanism of mutual entrainment should advance or delay the influence of one pacemaker on another, so that equality of IBI results. In the present study, we observed that, at a high coupling conductance ($G_c$ = 10 nS, Fig. 10 *A*) at which both 1:1 frequency entrainment and waveform entrainment occurred, the common interbeat interval was always intermediate between the two intrinsic values of IBI, and closer to that of the intrinsically faster pacemaker cell. This phenomenon was also observed in our recent publication (Wilders et al., 1996), in which we coupled two model SA node cells (Wilders et al., 1991), as well as a model SA node cell to a real SA node cell. This finding confirms the results of other experimental (Jalife, 1984; Anumonwo et al., 1991) and theoretical (Cai et al., 1994; Michaels et al., 1986; Ypey et al., 1980) studies. It should be noted, however, that the entrained interval measured in pairs of embryonic chick heart cells (DeHaan and Hirakow, 1972) and pairs of neonatal rat heart cells (Jongsma et al., 1987) was not always intermediate between the two intrinsic values of IBI. This discrepancy is most likely the result of differences in membrane currents that govern the process of diastolic depolarization in natural pacemaker cells compared with that in embryonic chick heart cells and pairs of neonatal rat heart cells.

The intrinsic rate at which pacemaker cells fire their action potentials depends to a large extent on the slope of diastolic depolarization. Therefore, we hypothesized that the decrease in depolarization rate of the intrinsically faster pacemaker cell (produced by the coupling current leaving this cell) would be equal to the increase in depolarization rate of the intrinsically slower cell (produced by the same coupling current entering this cell). To test this hypothesis, we introduced the diastolic depolarization time and found an excellent correlation between the observed common DDT and the predicted common DDT (Fig. 11). From these data, it again becomes clear that not only the intrinsically faster beating cell determines the synchronization rate, but also the intrinsically slower beating cell is of importance in determining the common IBI. These data suggest that the heart rate is the result of a "democratic" process underlying synchronous firing of SA node cells, with each cell contributing to the overall mutual entrainment, which was also suggested by Michaels et al. (1987), although the fastest cell seems to be more important in determining the common frequency than the slowest.

*Phasic and Tonic Interactions*

When two pacemakers are electrically coupled, the time-dependent variations in the potential difference between them separate the effects of one pacemaker cell on the other cell into two major components: (*a*) the relatively continuous "tonic" interactions of the pacemakers during diastolic depolarization, and (*b*) the "phasic" influence resulting from electrotonic current flow during the discharge of the action potential. The progressive changes in the strength of the phasic interactions at a $G_c$ of 0.1 nS (Fig. 2) results in 4:3 entrainment and resembles an atypical Wenckebach pattern of progressively increasing activation delay in a repetitive pattern. For the same cell pair, a $G_c$ of 0.2 nS (Fig. 4) resulted in a 1:1 frequency entrainment. At this low $G_c$, a depolarizing $I_c$ of ~14 pA flows from the intrinsically faster beating cell to the intrinsically slower beating cell after the activation of the intrinsically faster beating cell, such that the follower (intrinsically slower) cell fires its action potential with an ~50-ms latency. During diastolic depolarization, a tonic $I_c$ of ~2 pA flows from the intrinsically faster beating cell to the intrinsically slower beating cell without having an important effect on the diastolic depolarization rate of either cell. It can easily be understood that synchronization at low coupling conductances is governed by large differences in membrane potential between both cells; e.g., at the moment one cell fires its action potential and the other is still in the diastolic period. With stronger coupling ($G_c$ = 10 nS, Fig. 5), the phasic component becomes much shorter in duration and the depolarizing $I_c$ flowing from the intrinsically faster beating cell to the intrinsically slower beating cell during the action potential upstroke increases to values of 15–30 pA. However, the tonic period is prolonged and the tonic $I_c$ is increased approximately five times to ~9 pA (Figs. 5 and 9). Furthermore, during diastolic depolarization, membrane resistance is much higher (0.46 ± 0.12 GΩ [mean ± SD, $n$ = 10]) than the coupling resistance (0.1 GΩ, corresponding to a coupling conductance of 10 nS). Consequently, the increased tonic $I_c$, together with the high membrane resistance during diastole, will govern synchronization.

The major conclusions from our experimental observations is that at low $G_c$ mutual pacemaker synchronization results mainly from the phase-resetting effects of the action potential of one cell on the depolarization phase of the other. At high $G_c$, the tonic, diastolic interaction prevails. Michaels et al. (1986) used a "pulsed coupling" protocol in which coupling only occurred during the action potential. They showed that at low coupling conductances 1:1 entrainment was quantitatively similar to that obtained when coupling was continuous. This finding is in agreement with our finding that at low coupling conductances the phasic component is most important in pacemaker entrainment. The distinction between phasic and tonic interactions with regard to their contribution to synchronization at different levels of coupling has previously been made

(Ypey et al., 1980, 1982; Guevara, 1984; Wilders et al., 1996).

*Effects of Coupling Conductance on Membrane Ionic Current*

Figs. 8 and 9 demonstrate that the entrainment of the two cells by a rather high value of coupling conductance (10 nS) produces significant changes in the membrane ionic currents ($I_{ion}$) of each cell. By our definition of $I_{ion}$, this current is the net current produced by the membrane channels and electrogenic pumps of the cell. In the uncoupled state, this current is equal to $-C_m\, dV_m/dt$ and one can visualize a relationship such that the net membrane current therefore controls the time course of membrane potential. In the well coupled state, the different intrinsic action potential waveforms of the two cells are constrained to a common waveform, and thus this common waveform can be considered as an imposed waveform that has, in effect, voltage clamped each cell. During diastole in the coupled state, the rate of rise of potential has decreased for cell A (which had an intrinsically higher diastolic rate of rise) and increased for cell B (which had an intrinsically lower diastolic rate of rise). These alterations in the rate of rise of potential during diastole induce a more negative diastolic net membrane current for cell A and add a positive component to the net membrane current for cell B, which makes the net membrane current for cell B actually become positive during diastole. The positive net membrane current for cell B in the presence of a depolarizing membrane potential is not actually contradictory since the magnitude of the coupling current entering cell B during diastole is larger than the positive net membrane current of cell B during diastole. Similar arguments explain the alterations of net membrane current during the repolarization phases of the two cells.

The coupling current, $I_c$, which is plotted in Fig. 9 is positive during diastole. Note, however, that this coupling current is flowing out of cell A and into cell B because of our convention of treating the coupling current from cell A to cell B as a positive current. With respect to the individual cells, this coupling current indeed acts like an outward membrane current for cell A (which slows the intrinsic diastolic depolarization rate) and acts like an inward membrane current for cell B (which speeds up the intrinsic diastolic depolarization rate). Since the waveforms of the two cells and the capacitances of the two cells are nearly the same during the coupled state, we can approximately state that $C_{m,A}\, dV_{m,A}/dt = C_{m,B}\, dV_{m,B}/dt = -I_{ion,A} - I_c = -I_{ion,B} - I_c$ and, therefore, we derive that $I_{ion,A} - I_{ion,B} = -2I_c$ during the coupled state. Thus, the amount of coupling current required to make the two waveforms the same depends on the degree to which the membrane properties of the cells (which determine the net membrane current as a function of voltage and time for each cell) are different. For two cells with nearly identical membrane properties (defined as identical relationships of $I_{ion}$ as a function of voltage and time), the intrinsic waveforms of the two cells would be nearly identical to each other when uncoupled and would achieve frequency entrainment with a very small amount of coupling current. Conversely, the greater the differences in intrinsic membrane properties of the two cells when uncoupled, the more coupling current (and thus the more coupling conductance) is required for entrainment.

*Gap Junctions and Pacemaker Function*

In the rabbit SA node, gap junctions were identified at the electron microscopic level by Masson-Pévet et al. (1979). They estimated that the gap junctions occupy ~0–2% of leading SA node cell membrane. This raised some doubt about whether these very small junctional connections would be sufficient to maintain synchrony between pacemaker cells. Anumonwo et al. (1992) demonstrated the presence of gap junctions between SA node cells, which consist of the protein connexin43. They found that the conductance of a single SA nodal gap junctional channel ranged between 40 and 60 pS at room temperature. At 37°C, this single channel conductance would be ~75 pS (Bukauskas and Weingart, 1993). In the present study, we show that pacemaker synchronization occurs at a coupling conductance as low as 0.17 nS at a 26% difference in intrinsic IBI of two pacemaker cells (Fig. 10 *B*, Table II). This would mean that two to three gap junctional channels are sufficient for 1:1 frequency entrainment. A smaller difference in intrinsic IBI between both cells results in an even lower critical $G_c$. In a previous study (Wilders et al., 1996), in which we electrically coupled a single isolated SA node cell to the Wilders-Jongsma-van Ginneken model of an SA node cell (Wilders et al., 1991), we observed that at an IBI difference of ~10%, the critical $G_c$ became as low as 75 pS, corresponding to the conductance of a single gap junctional channel. Calculations performed by Noble (appendix to DeHaan, 1982) also indicate that two cells pacing at different frequencies could synchronize due to the presence of a single gap junctional conductance channel.

In a recent model study, Cai et al. (1994) described interactions between cells of a cell pair in which a "central" SA node cell with an IBI of 347 ms was coupled to a "peripheral" SA node cell with an IBI of 276 ms, thus having a difference in IBI of 26% when expressed as a percentage of the IBI of the intrinsically faster beating cell. The required coupling conductance for 1:1 frequency entrainment of 220 pS, which they modelled as comparable to the value of 150–170 pS, we determined from our experimental study, as well as the value of 180 pS predicted by our simulation results (Fig. 10 *B*).

In 10 isolated pairs of rabbit SA node cells, a mean cell-to-cell resistance of ~400 MΩ was observed (Anumonwo et al., 1992), corresponding with an intercellular coupling conductance of 2.5 nS. In the present study, we found that a $G_c$ of 2 nS resulted in almost complete frequency and waveform entrainment. In the same cell pair as used in Figs. 2–9, we observed at a $G_c$ of 2 nS a delay between the action potentials of only 3 ms. The action potential waveforms of the two cells closely resembled each other at this value of coupling conductance. This value of $G_c$ would necessitate ~30 gap junctional channels. In our experiments, the critical value of $G_c$ required for 1:1 frequency entrainment ranged between 150 and 300 pS, corresponding with two to four gap junctional channels. This implies that the coupling conductance required for both frequency and waveform entrainment of SA nodal cells is one order of magnitude higher than that required for frequency entrainment alone.

This work was supported in part by Netherlands Organization for Scientific Research grant 805–06–152, Netherlands Heart Foundation grant 92.310, and National Heart, Lung, and Blood Institute grant HL-22562.

*Original version received 31 July 1997 and accepted version received 6 October 1997.*

## REFERENCES

Anumonwo, J.M.B., M. Delmar, A. Vinet, D.C. Michaels, and J. Jalife. 1991. Phase resetting and entrainment of pacemaker activity in single sinus nodal cells. *Circ. Res.* 68:1138–1153.

Anumonwo, J.M.B., H.-Z. Wang, E. Trabka-Janik, B. Dunham, and R.D. Veenstra. 1992. Gap junctional channels in adult mammalian sinus nodal cells: immunolocalization and electrophysiology. *Circ. Res.* 71:229–239.

Bleeker, W.K., A.J.C. Mackaay, M.A. Masson-Pévet, L.N. Bouman, and A.E. Becker. 1980. Functional and morphological organization of the rabbit sinus node. *Circ. Res.* 46:11–22.

Bouman, L.N., and H.J. Jongsma. 1986. Structure and function of the sino-atrial node: a review. *Eur. Heart J.* 7:94–104.

Bouman, L.N., and H.J. Jongsma. 1995. The sinoatrial node: structure, inhomogeneity and intercellular interaction. *In* Pacemaker Activity and Intercellular Communication. J.D. Huizinga, editor. CRC Press, Inc., Boca Raton, FL. 37–50.

Bukauskas, F.F., and R. Weingart. 1993. Temperature dependence of gap junction properties in neonatal rat heart cells. *Pflügers. Arch.* 423:133–139.

Cai, D., R.L. Winslow, and D. Noble. 1994. Effects of gap junction conductance on dynamics of sinoatrial node cells: two cell and large scale networks. *IEEE Trans. Biomed. Eng.* 41:217–231.

Clapham, D.E., A. Shrier, and R.L. DeHaan. 1980. Junctional resistance and action potential delay between embryonic heart cell aggregates. *J. Gen. Physiol.* 75:633–654.

Clay, J.R., and R.L. DeHaan. 1979. Fluctuations in interbeat interval in rhythmic heart-cell clusters. *Biophys. J.* 28:377–390.

DeHaan, R.L. 1982. In vitro models of entrainment of cardiac cells. *In* Cardiac Rate and Rhythm. L.N. Bouman and H.J. Jongsma, editors. Martinus Nijhoff, The Hague, The Netherlands. 323–361.

DeHaan, R.L., and R. Hirakow. 1972. Synchronization of pulsation rates in isolated cardiac myocytes. *Exp. Cell Res.* 70:214–220.

Delmar, M., J. Jalife, and D.C. Michaels. 1986. Effects of changes in excitability and intercellular coupling on synchronization in the rabbit sino-atrial node. *J. Physiol. (Camb.)* 370:127–150.

de Maziére, A.M.G.L., A.C.G. van Ginneken, R. Wilders, H.J. Jongsma, and L.N. Bouman. 1992. Spatial and functional relationship between myocytes and fibroblasts in the rabbit sinoatrial node. *J. Mol. Cell. Cardiol.* 24:527–578.

Denyer, J.C., and H. Brown. 1987. A method for isolating rabbit sinoatrial node cells which maintains their natural shape. *Jpn. J. Physiol.* 37:963–965.

Denyer, J.C., and H. Brown. 1990. Rabbit sino-atrial node cells: isolation and electrophysiological properties. *J. Physiol. (Camb.).* 428: 405–424.

DiFrancesco, D., A. Ferroni, M. Mazzanti, and C. Tromba. 1986. Properties of the hyperpolarizing-activated current ($i_f$) in cells isolated from the rabbit sino-atrial node. *J. Physiol. (Camb.)* 377: 61–88.

Guevara, M.R. 1984. Chaotic Cardiac Dynamics (Ph.D. thesis). McGill University, Montreal, Quebec, Canada.

Honjo, H., M.R. Boyett, I. Kodama, and J. Toyama. 1996. Correlation between electrical activity and the size of rabbit sino-atrial node cells. *J. Physiol. (Camb.)* 496:795-808.

Irisawa, H., T. Nakayama, and A. Noma. 1987. Membrane currents of single cells from rabbit S-A and A-V nodes. *In* Electrophysiology of Single Cardiac Cells. D. Noble and T. Powell, editors. Academic Press Inc., Orlando, FL. 167–186.

Isenberg, G., and U. Klockner. 1982. Calcium tolerant ventricular myocytes prepared by preincubation in a "KB medium." *Pflügers. Arch.* 395:6–18.

Jalife, J. 1984. Mutual entrainment and electrical coupling as mechanisms for synchronous firing of rabbit sino-atrial pace-maker cells. *J. Physiol. (Camb.)* 356:221–243.

Jongsma, H.J., M.A. Masson-Pévet, and L. Tsjernina. 1987. The development of beat-rate synchronization of rat myocyte pairs in cell culture. *Basic Res. Cardiol.* 82:454–464.

Jongsma, H.J., J. Tsjernina, and J. de Bruijne. 1983. The establishment of regular beating in populations of pacemaker heart cells: a study with tissue-cultured rat heart cells. *J. Mol. Cell. Cardiol.* 15: 123–133.

Masson-Pévet, M.A., W.K. Bleeker, and D. Gros. 1979. The plasma membrane of leading pacemaker cells in the rabbit sinus node. *Circ. Res.* 45:621–629.

Michaels, D.C., E.P. Matyas, and J. Jalife. 1986. Dynamic interactions and mutual synchronization of sinoatrial node pacemaker cells. *Circ. Res.* 58:706–720.

Michaels, D.C., E.P. Matyas, and J. Jalife. 1987. Mechanisms of sinoatrial pacemaker synchronization: a new hypothesis. *Circ. Res.* 61:704–714.

Michaels, D.C., E.P. Matyas, and J. Jalife. 1990. Experimental and mathematical observations on pacemaker interactions as a mechanism of synchronization in the sinoatrial node. *In* Cardiac Elec-

trophysiology from Cell to Bedside. D.P. Zipes and J. Jalife, editors. W.B. Saunders Company, Philadelphia, PA. 182–192.

Nakayama, T., Y. Kurachi, A. Noma, and H. Irisawa. 1984. Action potential and membrane currents of single pacemaker cells of the rabbit heart. *Pflügers. Arch.* 402:248–257.

Nathan, R.D. 1986. Two electrophysiologically distinct types of cultured pacemaker cells from rabbit sino-atrial node. *Am. J. Physiol.* 250:H325–H329.

Noma, A., and N. Tsuboi. 1987. Dependence of junctional conductance on proton, calcium and magnesium ions in cardiac paired cells of guinea-pig. *J. Physiol. (Camb.)* 382:193–211.

Opthof, T. 1988. The mammalian sinoatrial node. *Cardiovasc. Drugs Ther.* 1:573–597.

Rae, J., K. Cooper, P. Gates, and M. Watsky. 1991. Low access resistance perforated patch recordings using amphotericin B. *J. Neurosci. Methods.* 37:15–26.

Rook, M.B., H.J. Jongsma, and A.C.G. van Ginneken. 1988. Properties of single gap junctional channels between isolated neonatal rat heart cells. *Am. J. Physiol.* 255:H770–H782.

Sano, T., T. Sawanobori, and H. Adaniya. 1978. Mechanism of rhythm determination among pacemaker cells of the mammalian sinus node. *Am. J. Physiol.* 235:H379–H384.

Scott, S. 1979. Stimulation Simulations of Young Yet Cultured Beating Hearts (Ph.D. thesis). State University of New York at Buffalo, Buffalo, NY.

Spray, D.C., and J.M. Burt. 1990. Structure–activity relations of the cardiac gap junction channel. *Am. J. Physiol.* 258:C195–C205.

Tan, R.C., and R.W. Joyner. 1990. Electrotonic influences on action potentials from isolated ventricular cells. *Circ. Res.* 67:1071–1081.

Verheijck, E.E., A.C.G. van Ginneken, J. Bourier, and L.N. Bouman. 1995. Effects of delayed rectifier current blockade by E-4031 on impulse generation in single sinoatrial nodal myocytes of the rabbit. *Circ. Res.* 76:607–617.

Wilders, R. 1993. From Single Channel Kinetics to Regular Beating: A Model Study of Cardiac Pacemaker Activity (Ph.D. thesis). University of Amsterdam, Amsterdam, The Netherlands.

Wilders, R., and H.J. Jongsma. 1993. Beating irregularity of single pacemaker cells isolated from the rabbit sinoatrial node. *Biophys. J.* 65:2601–2613.

Wilders, R., H.J. Jongsma, and A.C.G. van Ginneken. 1991. Pacemaker activity of the rabbit sinoatrial node: a comparison of mathematical models. *Biophys. J.* 60:1202–1216.

Wilders, R., E.E. Verheijck, R. Kumar, W.N. Goolsby, A.C.G. van Ginneken, R.W. Joyner, and H.J. Jongsma. 1996. Model clamp and its application to synchronization of rabbit sinoatrial node cells. *Am. J. Physiol.* 271:H2168–H2182.

Winfree, A.T. 1967. Biological rhythms and the behaviour of populations of coupled isolators. *J. Theor. Biol.* 16:15–42.

Ypey, D.L., D.E. Clapham, and R.L. DeHaan. 1979. Development of electrical coupling and action potential synchrony between paired aggregates of embryonic heart cells. *J. Membr. Biol.* 51:75–96.

Ypey, D.L., W.P.M. van Meerwijk, and R.L. DeHaan. 1982. Synchronization of cardiac pacemaker cells by electrical coupling: a study with embryonic heart cell aggregates and pacemaker cell models. *In* Cardiac Rate and Rhythm. L.N. Bouman and H.J. Jongsma, editors. Martinus Nijhoff, The Hague, The Netherlands. 363–395.

Ypey, D.L., W.P.M. van Meerwijk, C. Ince, and G. Groos. 1980. Mutual entrainment of two pacemaker cells. A study with an electronic parallel conductance model. *J. Theor. Biol.* 86:731–755.